AIAA JOURNAL
Vol. 37, No. 4, April 1999

Computational Aeroacoustics Simulations Using the Expansion About Incompressible Flow Approach

Scot A. Slimon*
Electric Boat Corporation, Groton, Connecticut 06340-4989
Marios C. Soteriou†
University of Connecticut, Storrs, Connecticut 06269
and
Donald W. Davis‡
Electric Boat Corporation, Groton, Connecticut 06340-4989

A series of two-dimensional numerical simulations is conducted in an effort to understand the behavior and validate the performance of a split hydrodynamic–acoustic computational aeroacoustics approach coupled with a specially tailored nonreflecting boundary condition. Validation cases considered include the classic aeroacoustic problem of the spinning vortex pair, the far-field aeolian tone prediction for a cylinder in crossflow, and the prediction of sound generation in a shear layer. In all cases good results are obtained based on comparisons with analytical solutions, experimental measurements, and direct numerical simulations. The split computational aeroacoustics approach is shown to be a cost-effective method for computing sound generation and propagation for a wide range of flows, including flows with noncompact source regions.

Nomenclature

Cp = pressure coefficient
D = cylinder diameter
f = frequency
M = Mach number
M_r = rotating Mach number
P = hydrodynamic pressure
p' = perturbation pressure
Re = Reynolds number
r_0 = rotation radius, vortex pair
Sr = Strouhal number
t = time
U_i = hydrodynamic velocity vector
u_i = velocity vector
u_i' = perturbation velocity vector
x_i = Cartesian coordinates
Γ = circulation
γ = specific heat ratio
ΔU = velocity difference across shear layer
δ = shear layer thickness
μ = dynamic viscosity
ρ_0 = ambient thermodynamic density
ρ_1 = hydrodynamic density
ρ' = perturbation density
σ = error function standard deviation
σ_{xi} = absorption coefficients in perfectly matched layer region

Introduction

THE relatively new field of computational aeroacoustics (CAA) has emerged over the past 10–15 years and holds promise in furthering the ability to predict and understand flow-generated sound. Although the CAA field has close ties to the field of computational fluid dynamics (CFD), the nature, characteristics, and objectives of aeroacoustic problems are distinctly different from those encountered in aerodynamics.[1–3] This point can be illustrated by considering sound radiated from a flow at low Mach numbers.[4] At a Mach number of 10^{-3}, the ratio of the radiated acoustic energy levels to source energy levels is on the order of 10^{-12}. In addition, the length scales associated with the propagating acoustic waves are significantly larger than those governing the near-field flow. These disparate energy levels and length scales require careful numerical treatment to avoid introducing spurious noise sources, excessive dissipation and dispersion of the acoustic quantities, and nonphysical wave reflection from computational boundaries. As such, the technology, e.g., solvers, algorithms, and boundary condition types, developed for CFD analyses is not always directly applicable to CAA.

Within the CAA field, several different approaches have been developed. Lighthill[1] has categorized these approaches into two groups. The first group, referred to as *direct simulation*, applies specially tailored CFD techniques over a large domain that includes the acoustic source region and extends out to the far field. For viscous flows, the direct simulation group makes use of direct numerical simulation (DNS), large-eddy simulation (LES), or time-averaged simulation of the Navier–Stokes equations to simultaneously compute the acoustic source generation and the resulting acoustic field radiation. Direct simulation involves an intense amount of computational effort due to the disparity in scales mentioned earlier, i.e., the computational prediction of aeroacoustic sources requires dense, highly stretched grids to resolve viscous gradients, whereas the prediction of acoustic wave propagation requires accurate prediction of small-amplitude quantities over large domains. The second group of approaches makes use of an acoustic analogy, e.g., Lighthill's acoustic analogy,[5] whereby CFD techniques are used to evaluate acoustic source strengths and distributions, and an acoustic wave equation is subsequently used to propagate acoustic quantities to the far field. To make use of these analogies, some approximations are typically made, such as assuming that the source terms can be adequately characterized by an incompressible flowfield. Despite such approximations, and because of the computational intensity associated with the direct simulation approach, Lighthill has recommended continued use of the acoustic analogy in one or more of its available forms.

Received July 15, 1998; revision received Nov. 28, 1998; accepted for publication Dec. 4, 1998.

*Principal Engineer, Department 414, Advanced Propulsion Plant Technology; also Ph.D. Candidate, Department of Mechanical Engineering, University of Connecticut, Storrs, CT 06269. Senior Member AIAA.

†Assistant Professor, Department of Mechanical Engineering. Member AIAA.

‡Principal Engineer, Department 464, Fluid Mechanics. Senior Member AIAA.

Recently, Hardin and Pope[6] introduced a CAA scheme called *expansion about incompressible flow* (EIF). The EIF approach is similar to the approximate acoustic analogies in that it splits the direct simulation approach into an incompressible flow problem and a perturbation problem and does not allow for acoustic backscatter into the flow solution. In the near field, the perturbation quantities are the difference between the compressible and incompressible flowfield variables. The perturbation quantities are equivalent to acoustic quantities in the far field. The splitting used in the EIF approach is intended to simplify the difficulties associated with resolving the small amplitude of acoustic wave fluctuations relative to the mean flow quantities, the long propagation distance out to the far field, and the disparate acoustic and viscous length scales. In addition, optimum numerical schemes can be applied to the equation sets governing each problem; implicit schemes can be used for the incompressible equations, and explicit schemes can be used for the perturbation equations. The split approach also provides flexibility in specifying the type and location of boundary conditions; i.e., acoustic/perturbation boundary conditions can be specified at different locations relative to the boundary conditions specified for the incompressible equations. In contrast to the more sophisticated acoustic analogy equations, e.g., Phillips's equation[7] and Lilley's equation,[8] the EIF approach accounts for flow–acoustic interaction in an unambiguous fashion. In these equations, the acoustic wave operator is constructed in such a way as to closely resemble the linearized moving-medium wave equation. This is not completely physical because some of the terms used to construct the wave operator may be important in the sound generation process but do not appear as source terms.[9] This ambiguity in segregating the flow–acoustic interaction terms from sound generation source terms results from the nonlinearity of the governing equations. Because the EIF approach separates the flow variables into acoustic and hydrodynamic parts, the source terms can be unambiguously segregated from terms that process the acoustic waves. As such, the EIF approach should provide an effective method of predicting acoustic fields resulting from low-Mach-number, noncompact source regions.

To date, the EIF approach has undergone limited validation, and all of the validation cases considered have involved compact acoustic source regions.[6,10,11] In the present work, validation of the EIF approach is extended through the computation of the acoustic fields associated with three different unsteady flowfields: the spinning vortex pair, flow past a circular cylinder, and a forced planar shear layer. The spinning vortex pair is a particularly useful first validation case because the incompressible and acoustic far-field solutions can be obtained analytically. Consequently, because hydrodynamic solutions need not be numerically computed for each new acoustic solution, acoustic solver modifications and alternative boundary condition types can be tested efficiently. The use of the cylinder in crossflow as a second validation case is a logical progression from the spinning vortex pair because this problem requires numerical computation of the hydrodynamic source terms. As such, it represents a complete test of the coupled hydrodynamic and acoustic solvers. The acoustic fields for both the spinning vortex pair and the cylinder in crossflow are simulated in the present study at relatively low Mach numbers such that each of these validation cases is characterized by compact acoustic source regions. In contrast, the forced planar shear layer is characterized by an extensive region of convecting vortices. Because of this, the mixing layer was selected as a third validation case since it tests the ability of the EIF approach to predict sound generation and propagation resulting from noncompact acoustic sources.

Numerical Model

Governing Equations

In the EIF approach, the compressible flowfield is separated into an incompressible, viscous hydrodynamic flowfield and an inviscid, acoustic perturbation field. Recently, we have shown that equations governing the hydrodynamic and acoustic fields can be developed by performing a Mach number M expansion of the fully compressible Navier–Stokes equations.[12] The incompressible equations are obtained by neglecting $\mathcal{O}(M^2)$ terms and higher. The acoustic perturbation equations are obtained by subtracting the incompressible equation set from the expanded fully compressible flow equations and by neglecting viscous action on the perturbation quantities. An assumption implicit in the EIF approach is that the acoustic or perturbation field has no effect on the incompressible flowfield because $\mathcal{O}(M^2)$ terms are neglected in the incompressible flow equations. The resulting set of equations, assuming a Newtonian fluid and an isothermal thermodynamic field, can be expressed in nondimensional tensor notation form as follows.

Incompressible, viscous equations:

$$\frac{\partial U_i}{\partial x_i} = 0 \tag{1a}$$

$$\frac{\partial U_i}{\partial t} + U_j \frac{\partial U_i}{\partial x_j} = -\frac{\partial P}{\partial x_i} - \frac{1}{Re}\frac{\partial}{\partial x_j}\left(\frac{\partial U_i}{\partial x_j}\right) \tag{1b}$$

Inviscid, perturbation equations:

$$\frac{\partial \rho'}{\partial t} + \frac{\partial}{\partial x_i}[(1+\rho_1+\rho')u_i' + \rho' U_i] = -\frac{\partial \rho_1}{\partial t} - U_i \frac{\partial \rho_1}{\partial x_i} \tag{2a}$$

$$\begin{aligned}\frac{\partial}{\partial t}[(1+\rho_1+\rho')u_i' + \rho' U_i] + \frac{\partial}{\partial x_j}[(1+\rho_1)(U_i u_j' + U_j u_i' + u_i' u_j')] \\ + \frac{\partial}{\partial x_j}[\rho'(U_i U_j + U_i u_j' + U_j u_i' + u_i' u_j')] + \frac{\partial p'}{\partial x_i} \\ = -\frac{\partial(\rho_1 U_i)}{\partial t} - \frac{\partial(\rho_1 U_i U_j)}{\partial x_j}\end{aligned} \tag{2b}$$

where the primed lowercase quantities in the perturbation equations represent the acoustic variables. Each of the governing equations has been nondimensionalized using U_0 for velocity, ρ_0 for ρ, $\rho_0 U_0^2$ for pressure, L_0 for length, and L_0/U_0 for time. A relation between ρ_1 and P and between ρ' and p' can be established by combining Mach number expansions of the equation of state and energy equation:

$$\frac{\mathrm{D}\rho_1}{\mathrm{D}t} = M^2 \frac{\mathrm{D}P}{\mathrm{D}t} \tag{3}$$

$$\frac{\mathrm{D}\rho'}{\mathrm{D}t} = M^2 \frac{\mathrm{D}p'}{\mathrm{D}t} - \left(\frac{\gamma-1}{2}\right)\frac{\mathrm{D}\left(\rho_1^2\right)}{\mathrm{D}t} \tag{4}$$

In the development of Eqs. (3) and (4), heat conduction and viscous dissipation have been neglected. These equations differ somewhat from those used in previous investigations.[6,10,11] Formal development of Eqs. (1–4) is provided in Ref. 12.

Numerical Methodology

The strategy of the overall hydrodynamic–acoustic approach can be illustrated by considering the low-Mach-number flow of Fig. 1, which shows an unsteady near-field flow region resulting in acoustic radiation to the far field. The near-field region is characterized by dimensions based on the hydrodynamic scales of the flow. In contrast, the far-field region is characterized by dimensions based on the acoustic wavelengths for each frequency of interest. Resolution of the viscous scales of the hydrodynamic flow using a finite difference approach requires a dense computational grid with high stretching to optimize the number and distribution of grid points. Optimum resolution of the propagating acoustic waves would make use of a uniform grid that extends many wavelengths out to the far-field boundary. By splitting the hydrodynamic and acoustic solutions, and by neglecting the viscous terms in the acoustic equation, the EIF approach accommodates the different discretization requirements resulting from the disparate length scales. In addition, this approach allows for specification of different boundary condition types and locations for the near-field and far-field quantities. Figure 1 is used to illustrate this point; the hydrodynamic inlet boundary can be specified with a fixed velocity profile (representative of a known boundary layer or freestream velocity profile), whereas the far-field acoustic boundary could be specified with nonreflecting boundary conditions (representative of acoustic radiation in an unbounded physical space) located some distance away from the hydrodynamic inlet. Two solvers, an incompressible flow solver and a perturbation

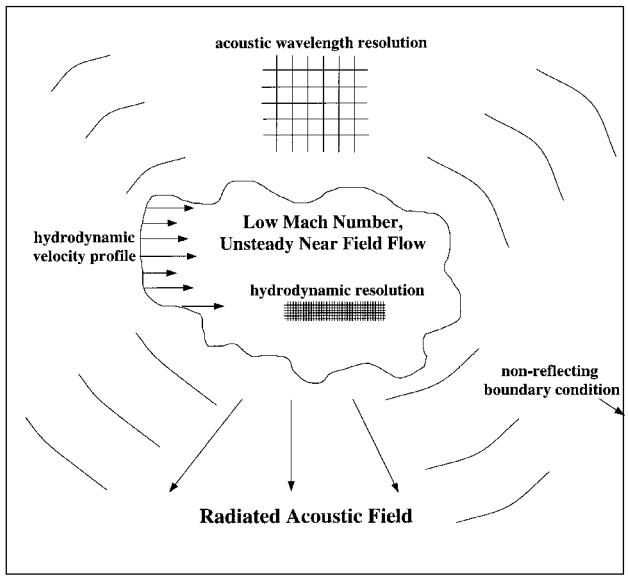

Fig. 1 Schematic of acoustic radiation from a low-Mach-number source region, as well as some numerical simulation considerations.

equation solver, are used to compute the hydrodynamic and acoustic fields, respectively, as described in the following.

Incompressible Flow Solver

The incompressible Navier–Stokes solver, NFC,[13–15] used for the solution of Eqs. (2a) and (2b), is finite difference based and uses pseudocompressibility and a Briley–McDonald linearized block implicit-type alternating-direction implicit scheme. The solver is fully vectorized and parallelized for maximum performance on coarse grain parallel vector-processor machines. The governing equations are cast in primitive variable form using a pseudocompressibility term in the continuity equation to efficiently link the updates of the velocity and pressure fields. The resulting system of conservation equations is transformed to generalized curvilinear coordinates and is discretized using finite differences (central spatial differencing and full nonorthogonal viscous terms). A hybrid second- and fourth-order, implicit and explicit artificial dissipation scheme is used to enhance solution stability. All artificial dissipation is applied locally and is adjusted each time step based on nodal checks of grid quality and solution stability obtained from grid cell Reynolds number and local eigenvalues. With this approach, dissipation levels are established for optimum solution convergence behavior and solution quality.

Time-accurate solutions are obtained with the incompressible solver using a subiteration approach,[16] which extends the pseudocompressibility method to time-accurate incompressible flows by subiterating each physical time step to drive the divergence of velocity to zero. The time derivatives in the momentum equations are computed for each physical time step and appear as source terms on the right-hand side. Based on a series of convergence tests using this approach, it was found that extrapolating new values of the velocity field after each physical time step could reduce the required number of subiterations. The improvement in convergence using this extrapolation procedure is, however, problem dependent and, therefore, requires evaluation for each computed flowfield. Nevertheless, this additional effort has proven worthwhile because a significant number of time steps are generally required to get reasonable spectral resolution in the acoustic simulations.

Acoustic Perturbation Equation Solver

The acoustic perturbation equations [Eqs. (2)] are solved with an explicit, 2–2 MacCormack[17] scheme using a generalized body-fitted coordinate system. Use of an explicit scheme provides the best approach for the solution of the acoustic perturbation equations. Although an implicit scheme could be used, the high Courant–Friedrichs–Lewy (CFL) numbers allowed with such schemes would introduce dissipation and dispersion into the solution. Because CFL numbers close to one are preferred to minimize these numerical errors, and because explicit algorithms can be used at CFL numbers approaching one, the use of an explicit scheme provides the simplest and least expensive approach for the acoustic solution. Depending on the problem, the time-step limit based on CFL requirements for the acoustic solver can be smaller or larger than the optimum time step based on convergence requirements for the incompressible solver. Therefore, the most efficient solution scheme would advance each solution (incompressible and acoustic) at the maximum time step allowed. If the incompressible time step is larger than the acoustic time step, the acoustic source terms derived from the incompressible solution are interpolated in time between two successive incompressible time steps. The hydrodynamic source terms that appear in the acoustic equations are computed on the hydrodynamic grid and interpolated in space onto the acoustic grid using bilinear functions. This is done because the acoustic grid points can be distributed differently than the hydrodynamic grid points. For example, the spacing in the acoustic grid can be significantly larger than the spacing in the near-wall regions of the hydrodynamic grid. To facilitate the interpolation, a map file, which contains the coefficients used in the interpolation scheme, is generated prior to performing coupled hydrodynamic–acoustic calculations. Although the chosen numerical scheme does not inherently require the addition of explicit damping terms, initial testing revealed that fourth-order smoothing was required to control oscillations in regions with large hydrodynamic source terms.

A radiation boundary condition has been implemented in the perturbation equation solver to minimize contamination of the solution by artificial reflections from the computational boundaries. In this work, the perfectly matched layer (PML) absorbing condition, developed by Berenger[18] for the Maxwell equations and by Hu[19] for the nonlinear and linearized Euler equations, has been extended to the EIF equations. For the PML absorbing condition, regions adjacent to the outflow boundaries of the acoustic computational domain are discretized using 15–20 grid points. In these regions, a PML equation set is constructed such that the outgoing waves are absorbed. The PML equations are constructed by splitting each of the flow variables, e.g., ρ' is split into ρ'_1 and ρ'_2, and by segregating spatial gradients into each split equation, e.g., the ρ'_1 equation only includes x_1 gradients. The PML equations include absorption coefficients, σ_{x1} and σ_{x2}, which are used to damp out waves normal to the x_1 and x_2 axes, respectively. These absorption coefficients are increased exponentially across the PML region to gradually absorb the outgoing waves. Using this approach, both Berenger[18] and Hu[19] have shown that the PML approach is perfectly absorbing for plane waves at any incidence angle and frequency. The hydrodynamic source terms involving spatial gradients of the incompressible quantities are split in the same fashion as described earlier for the acoustic variables. Based on a series of tests, it was found that optimum performance of the PML absorbing condition was obtained when the source terms involving time gradients of the incompressible quantities were split equally between the split equations. In addition, rather than linearize the PML equations through the specification of a pseudomean flow (as was done by Hu for the nonlinear form of the Euler equations), a nonlinear form of the PML equations for the EIF approach has been developed. This is illustrated for the x_1-momentum equation

$$\frac{\partial \varphi}{\partial t} + \frac{\partial}{\partial x_1}[\varphi(U_1 + u'_1) + (1+\rho_1)U_1 u'_1 + p'] + \frac{\partial}{\partial x_2}[\varphi(U_2 + u'_2) + (1+\rho_1)U_1 u'_2] = -\frac{\partial(\rho_1 U_1)}{\partial t} - \frac{\partial\left(\rho_1 U_1^2\right)}{\partial x_1} - \frac{\partial(\rho_1 U_1 U_2)}{\partial x_2} \tag{5a}$$

which is split in the PML region,

$$\frac{\partial \varphi_1}{\partial t} + \sigma_{x1}\varphi_1 + \frac{\partial}{\partial x_1}[\varphi_1(U_1 + u'_1) + (1+\rho_1)U_1 u'_1 + p'] = -\frac{1}{2}\frac{\partial(\rho_1 U_1)}{\partial t} - \frac{\partial\left(\rho_1 U_1^2\right)}{\partial x_1} \tag{5b}$$

$$\frac{\partial \varphi_2}{\partial t} + \sigma_{x2}\varphi_2 + \frac{\partial}{\partial x_2}[\varphi_2(U_2 + u_2') + (1+\rho_1)U_1 u_2'] = -\frac{1}{2}\frac{\partial(\rho_1 U_1)}{\partial t} - \frac{\partial(\rho_1 U_1 U_2)}{\partial x_2} \quad (5c)$$

where $\varphi = (1 + \rho_1 + \rho')u_1' + \rho' U_1 = \varphi_1 + \varphi_2$.

Results and Discussion

Spinning Vortex Pair

The spinning vortex pair configuration consists of two corotating vortices separated by a finite distance, as shown in Fig. 2. This particular problem has been used for validation of several aeroacoustic codes.[11,20] The far-field solution has been determined by Müller and Obermeier,[21] who solved the problem using the method of matched asymptotic expansions (MAE). In this method, the solution of the incompressible equation set is matched with the solution of the acoustic equation set in some intermediate domain. As such, the MAE solution provides both a hydrodynamic solution that can be used to compute source terms for the perturbation equations set and an acoustic solution for comparison with the predicted acoustic field.

The acoustic solution was computed on a rectangular domain using a uniform grid with 19,881 uniformly spaced grid points ($\Delta x_i = 2r_0$). The flow and acoustic parameters were selected to be consistent with those of one of the simulations performed by Lee and Koo,[11] i.e., $M_r = 0.0477$ and $\Gamma = 0.6$. The hydrodynamic field was determined from the near-field MAE solution and was used to compute the source terms at each acoustic grid point. The acoustic solution was computed for 11 periods (one period corresponds to one complete revolution of the vortex pair) using $\Delta t = 0.006$. This time step resulted in a CFL number of 0.9. Figure 3 shows the computed acoustic density field over the entire domain, including the PML region. The acoustic field has a spinning, double-spiral pattern consistent with the analytical solution and the solutions reported in previous investigations.[11,20] The PML regions appear to successfully eliminate reflections from the far-field boundaries. Figure 4 provides a comparison of the computed and analytical acoustic pressure along the diagonal, i.e., the line $x_1 = x_2$, of the acoustic grid and shows that the EIF predicted acoustic field has the correct wavelength and amplitude. Figure 4 also shows results using three different maximum values for the absorption coefficients (σ_{x1}, σ_{x2}) in the PML region. The solutions are virtually identical in the computational domain, whereas in the PML region, the higher absorption coefficients damp the outgoing waves at a faster rate. The EIF acoustic solution for the spinning vortex problem was computed using less than 5 CPU minutes on a Cray C90. The numerical accuracy of the computations was assessed by performing a grid refinement study. Four different grids with uniform spacing of $\Delta x_i = 6r_0$, $\Delta x_i = 3r_0$, $\Delta x_i = 2r_0$, and $\Delta x_i = 1.5r_0$ were used in this assessment. The solution was seen to be effectively grid independent, i.e., the amplitude of the far-field acoustic pressure oscillations varied less than 1%, for $\Delta x_i < 3r_0$. This grid spacing corresponds to a resolution of approximately 20 points per wavelength. Based on this, a minimum criterion of 25 points per wavelength was established and was used for the other validation cases reported in this paper.

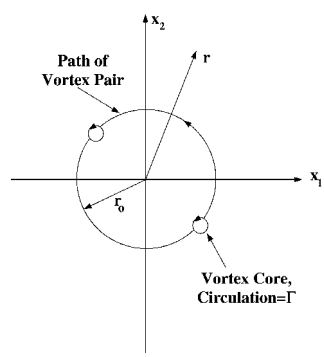

Fig. 2 Spinning vortex pair configuration.

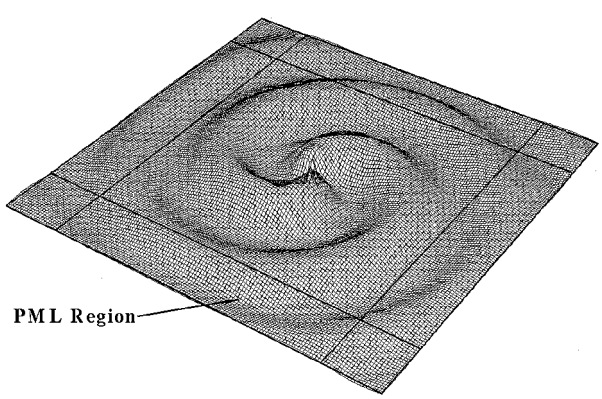

Fig. 3 Spinning vortex pair; acoustic density field. Computational grid is deformed by 10^3 times the acoustic density field, which ranges between -3×10^{-5} and 3×10^{-5}. Dark lines outline the PML region.

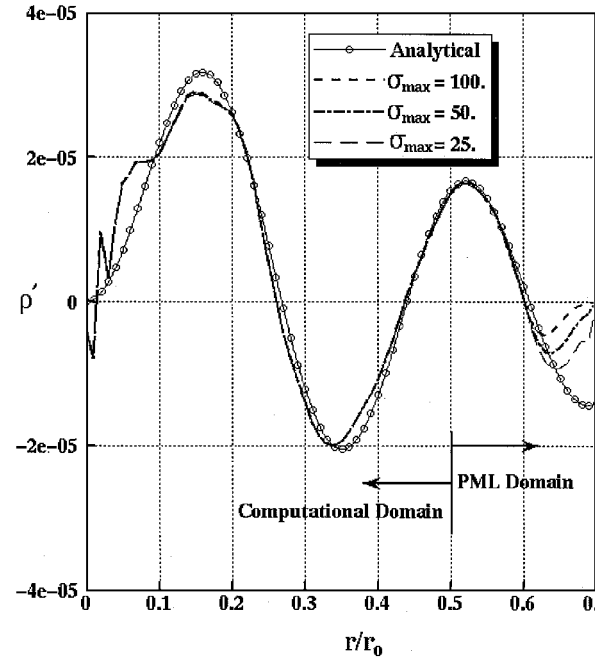

Fig. 4 Spinning vortex pair; comparison of computed and MAE predicted acoustic pressure along the diagonal line $x_1 = x_2$.

Cylinder in Crossflow

Blake[22] describes the subsonic flow-induced noise generation due to flow past a circular cylinder as being one of the most investigated topics in aeroacoustics. This sound generation process is relevant to flow past an automobile antenna as well as airframe noise and was recently used as a CAA benchmark problem.[23] Experimental data in the form of far-field sound pressure levels are available for comparison and were taken at a Reynolds number of 9×10^4 and a Mach number of 0.2 (Ref. 24). Several methods have been used in previous investigations to solve the hydrodynamic and acoustic portions of this problem.[25–27] Hydrodynamic solutions included Reynolds-averaged Navier–Stokes simulations, LES, and DNS. Three different acoustic analogies, including those due to Lighthill,[5] Curle,[28] and Ffowcs Williams and Hawkings,[29] were used to predict the corresponding acoustic fields.

In the present work, the hydrodynamic solution was computed at the same Reynolds number as the aforementioned experiment. The hydrodynamic domain, which was nondimensionalized using the cylinder diameter D, extended $15D$ above and below and $15D$ in front of and $35D$ behind the cylinder. A total of 35,046 grid points in 12 blocks were used to discretize the domain using a grid spacing of $0.0002D$ adjacent to the cylinder wall. The hydrodynamic solution was computed for 1000 time steps using $\Delta t = 0.1$, with 10

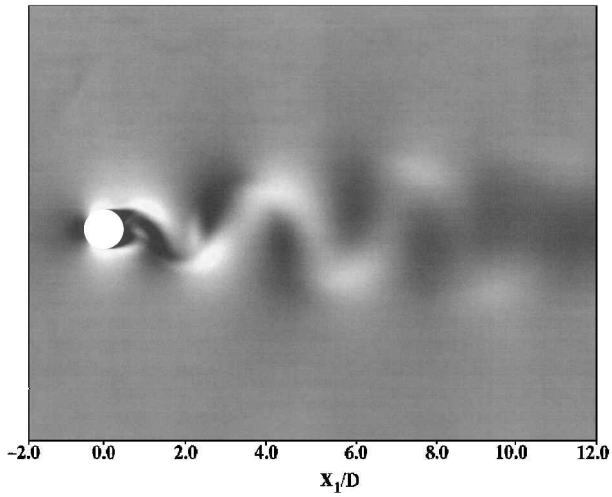

Fig. 5 Cylinder in crossflow; velocity magnitude contours. Contours range between 0.0 and 1.8, and dark shading represents low velocities.

subiterations per time step to establish an incompressible, stationary flow. Figure 5 shows the predicted velocity magnitude contours after 1000 time steps. The solution exhibited periodic shedding from the cylinder at a peak Strouhal number Sr of 0.230, which is in the range of predicted frequencies reported by previous investigations[25–27] but is somewhat higher than the experimental value of $Sr = 0.190$.

The acoustic domain, which was significantly larger than the hydrodynamic domain, extended $136D$ above, $45D$ below, $75D$ in front of, and $136D$ behind the cylinder. The acoustic grid used 156,071 grid points with a grid spacing (away from the wall) of $0.5D$. This grid spacing corresponds to a resolution of 25 points per wavelength for the drag harmonic. Two approaches were used in the acoustic solution to simulate the freejet used in the experimental setup[24]: 1) The cylinder was held stationary in a moving medium, which extended to the far field. 2) The cylinder was moved in a quiescent field. For both of these approaches, the hydrodynamic solution simulated a stationary cylinder in a moving medium. In approach 2, the freestream velocity was subtracted from the hydrodynamic solution prior to computing the hydrodynamic source terms used in the acoustic solution. Over 30 cycles of the drag harmonic were computed using $\Delta t = 0.02$, which corresponds to a CFL number of approximately 0.7. Figure 6 provides the predicted acoustic density fields using the two acoustic solution approaches. As shown in Fig. 6, the convective contributions of the mean flow have a significant effect on the directivity of the acoustic density field. Relative to the stationary cylinder results, the moving cylinder solution does not exhibit a Doppler shift of the drag harmonic in front of the cylinder. (The acoustic waves are propagating in a stationary acoustic medium.) The opposite effect is seen in the wake of the cylinder. In addition, the peak in the lift harmonic is shifted toward the downstream direction for the stationary cylinder case. Figure 7 compares the far-field directivity pattern of the normalized sound pressure levels computed using approaches 1 and 2 to the experimental data. The directivity pattern for the translating cylinder solution compares very well with the experimental results, except for the last two data points near the cylinder horizontal axis. In contrast, the stationary cylinder compares reasonably well with the data in this region but predicts the peak sound pressure level at approximately 75 deg relative to the cylinder horizontal axis. These results appear reasonable because the experiment used a jet to establish the flow past the cylinder, such that much of the acoustic wave propagation was through a quiescent medium. Therefore, the translating cylinder solution would be more representative of the experiment away from the horizontal cylinder axis, and the stationary cylinder solution would be more representative of the experiment near the horizontal cylinder axis. The computed sound pressure level was 11–12 dB higher than the experimentally measured levels directly above the cylinder. Similar differences were observed in previous investigations[25–27] and have been attributed to the two-dimensional approximation of the hydrodynamic flowfield.[25] This approximation

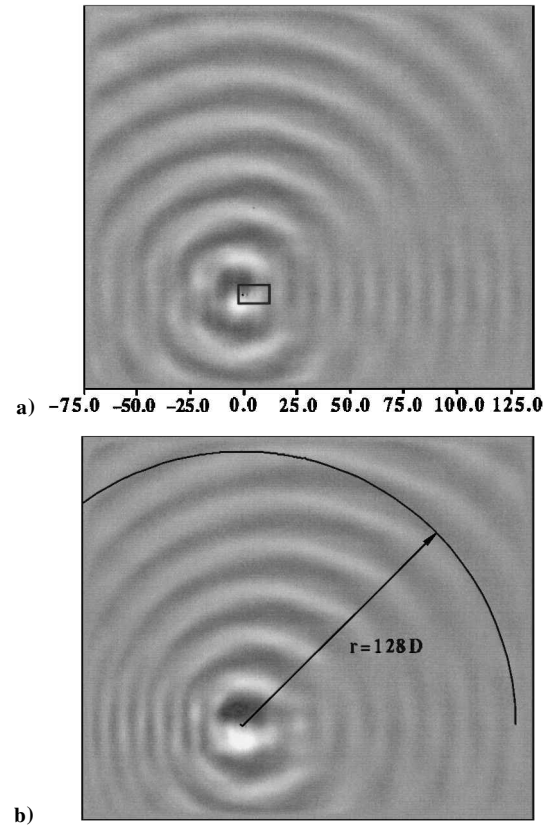

Fig. 6 Cylinder in crossflow; acoustic density contours (ranging between -2×10^{-3} and 2×10^{-3}) for a) stationary cylinder case (rectangle represents the hydrodynamic domain shown in Fig. 5) and b) translating cylinder case. (Indicated radius is used for directivity sampling in Fig. 7.)

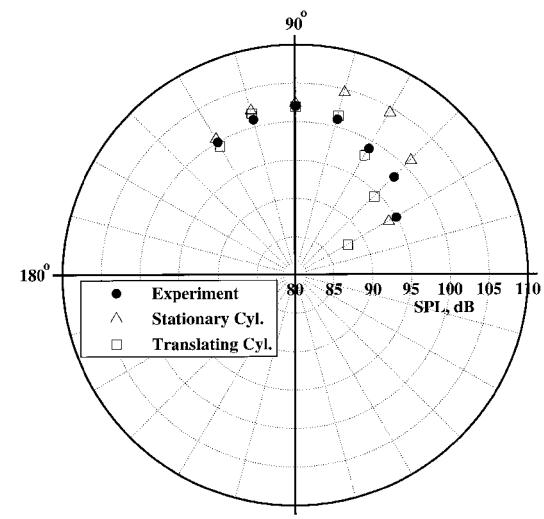

Fig. 7 Cylinder in crossflow; directivity pattern of acoustic pressure at $r/D = 128$.

implicitly assumes that vortex shedding is coherent over the entire length of the cylinder. In addition, the two-dimensional acoustic calculation does not allow the acoustic field to spread in the x_3 direction, resulting in overpredicted acoustic levels. The EIF acoustic solution for the cylinder in crossflow was computed using approximately 4 CPU hours on a Cray C90.

Shear Layer

Shear layers are created by the merging, downstream of a splitter plate or bluff body, of two streams of unequal velocity. Experimental evidence suggests that the flowfield resulting from this merging is

essentially two dimensional at its early stages and is dominated by coherent vortical structures. These structures are a manifestation of the Kelvin–Helmholtz instability and control the subsequent growth of the layer via their mutual interactions. Shear layers, together with jets and wakes, have attracted substantial experimental[30–32] and computational[33–35] attention because they provide canonical representations of more complicated shear flows. Noise generation by shear flows has also been the subject of several investigations. For example, Laufer and Yen[36] carried out measurements of noise generated by a forced jet. Despite the low Mach number of the flow, i.e., $0.05 < M < 0.20$, the acoustic radiation exhibited a highly directional character. Crighton and Huerre[37] have classified such acoustic fields as being superdirective and have shown that the hydrodynamic pressure field resulting from the convecting vortices generated by the shear layer has the form of a traveling subsonic plane wave packet. The amplitude of the wave is modulated by some global envelope function. Crighton and Huerre[37] have analytically shown that the hydrodynamic near field resulting from this modulated wave packet is noncompact, even for low-Mach-number flows. Colonius et al.[38] have performed DNS computations of the compressible Navier–Stokes equations in their investigation of sound generation in a forced planar mixing layer. The computational domain included both the near-field region and a portion of the acoustic field. In addition, they computed the acoustic field using Lilley's equation, with source terms generated from the DNS results. In both of these approaches, a superdirective acoustic field was predicted consistent with the noted experimental and analytical findings.

In the present study, the flow and resulting sound generation and propagation due to a forced planar shear layer were simulated using the EIF approach. The flow parameters used in this simulation were consistent with those used in Ref. 38, i.e., $Re = \rho \Delta U \delta / \mu = 250$ and $M = 0.5$ and 0.25 for the high- and low-speed flow streams, respectively. The hydrodynamic grid extended approximately 500δ in the x_1 direction and 15δ in the x_2 direction. A single block grid was used with 730 points along x_1 and 161 points along x_2. The grid is clustered toward the centerline ($x_2 = 0$) of the shear layer with a minimum grid spacing of 0.04δ. The hydrodynamic inlet velocity profile was specified using an error function profile as given by

$$u_2(x_2, t) = (u_{\text{av}}/2) + (\Delta U/2)[\text{erf}(x_2/\sigma)] \tag{6}$$

where u_{av} is the average of the high- and low-speed stream velocities. Forcing was applied at the fundamental f_1 and first subharmonic frequencies f_2 obtained using linear stability analysis[39] and was imposed by specifying an oscillating vertical component of velocity, u_2, at the inlet boundary of the hydrodynamic domain using $u_2 = A[\sin(2\pi f_1 t) + \sin(2\pi f_2 t)]$. The amplitude A was selected as $0.0002\Delta U$ based on a series of tests, which showed that this level of inlet forcing was large enough to cause the vortices to roll up in a reasonable distance yet small enough so that it did not result in a highly compact, dominant acoustic source. In this way, the most significant acoustic sources were located well downstream of the inlet forcing location and were due to the dynamic behavior, e.g., rollup, saturation, etc., of the vortices. Damping was explicitly added to the right-hand side of the incompressible flow solver between $x_1/\delta = 220$ and $x_1/\delta = 500$ to eliminate vortices exiting the outlet boundary of the hydrodynamic domain. This was done because a constant pressure was specified at the outlet boundary condition. Any disturbances exiting this boundary would cause the entire pressure field to oscillate unnaturally and thereby introduce erroneous forcing of the acoustic solution. After several hundred iterations, the hydrodynamic field evolved to a stationary solution consisting of a series of convecting vortices, as seen in the vorticity field shown in Fig. 8. The pressure coefficient Cp at several different instances in time is shown in Fig. 9 along x_1 for $x_2 = 0$. The pressure field has a form similar to that described by Crighton and Huerre[37] and computed by Colonius et al.,[38] i.e., the pressure oscillations form an essentially stationary wave packet with amplitude variation in space. Oscillations in the pressure field due to the convecting vortices are seen to dissipate rapidly for $x_1/\delta > 220$ as a result of the explicit damping.

The acoustic domain was designed such that the computational grid extended above and below the hydrodynamic domain five acoustic wavelengths of the subharmonic frequency. In addition, 25 points per wavelength were used to resolve the fundamental frequency. This resulted in 80,571 grid points with a uniform grid spacing of 0.145δ. The combined hydrodynamic–acoustic simulation was started once the hydrodynamic solution became stationary. Over 100 periods of the subharmonic frequency were computed using $\Delta t = 0.02$, which corresponds to a CFL number of approximately 0.8. To mitigate the effects of the rapid damping in the hydrodynamic solution (see Fig. 9 for $x_1/\delta > 220$), the source terms and incompressible variables used in the acoustic solution were gradually decayed between $x_1/\delta = 145$ and $x_1/\delta = 220$ using a linear decay function. These variables were also decayed near the inlet to reduce the effect of forcing the incompressible flow on the acoustic solution. The acoustic density field resulting from the unsteady hydrodynamic flowfield is shown in Fig. 10. Also shown in Fig. 10 are contours of the hydrodynamic density, which have been imprinted

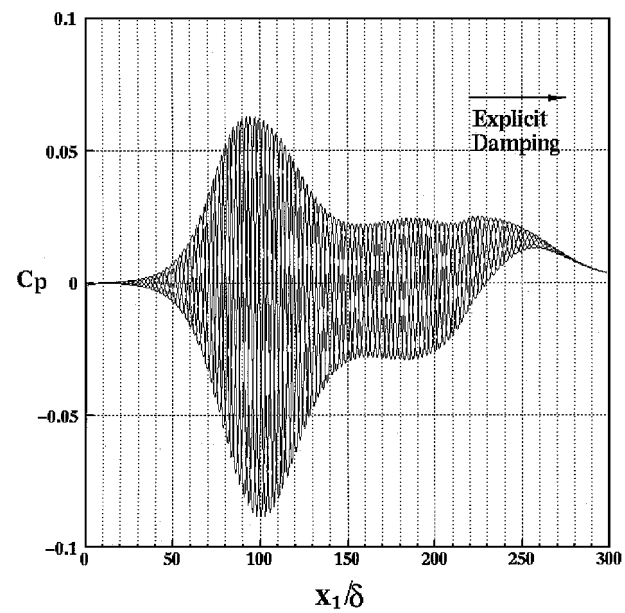

Fig. 9 Shear layer; pressure coefficient along $x_2 = 0$. Explicit damping was used to damp the oscillations for $x_1/\delta = 220$.

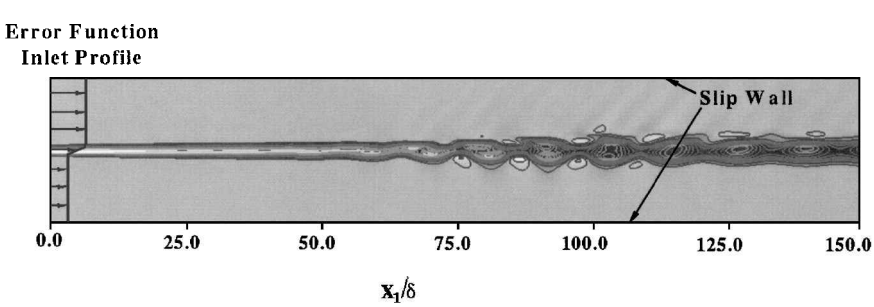

Fig. 8 Shear layer; vorticity contours. Contours range between − 0.25 and 0.025, dark shading represents regions of high vorticity, and contour lines are inverted to highlight vorticity field (light contour lines indicate high vorticity).

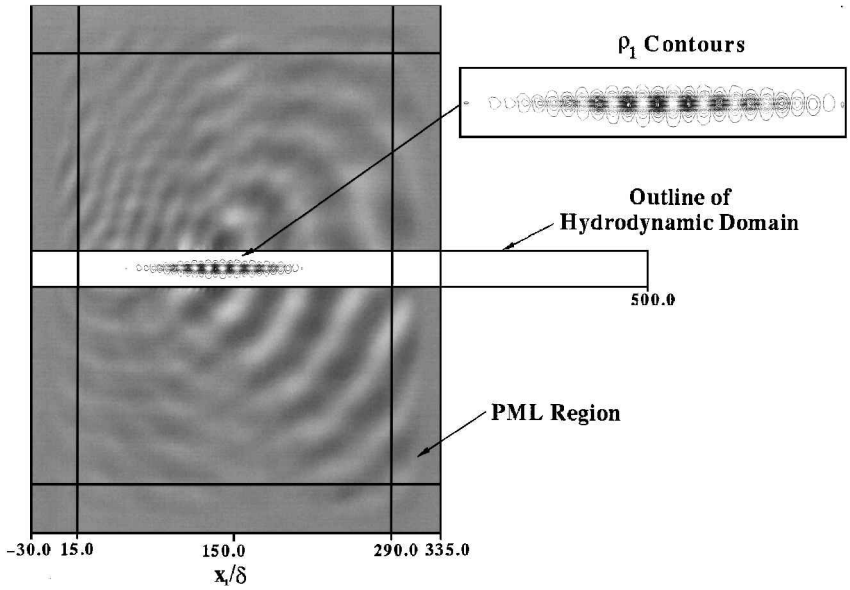

Fig. 10 Shear layer; acoustic density contours. Contours range between -2.5×10^{-6} and 2.5×10^{-6}. Hydrodynamic density contours lines are shown in the shear layer region and range between -0.8×10^{-2} and 0.6×10^{-2} at intervals of 0.1×10^{-2}.

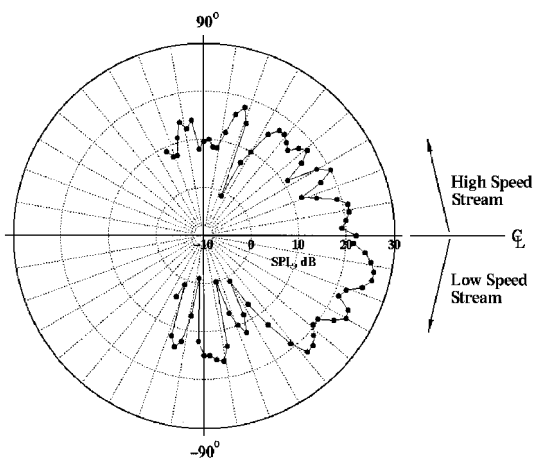

Fig. 11 Shear layer; directivity pattern: sound pressure level (SPL).

onto the acoustic domain and were used in the acoustic computations. The contours of acoustic density range between -2.5×10^{-6} and 2.5×10^{-6}. The directivity of the acoustic field at the subharmonic frequency is shown in Fig. 11 and was determined by computing sound pressure levels every 3 deg on a circular arc with radius $r/\delta = 200$, centered before the peak of the hydrodynamic pressure oscillations ($x_1/\delta = 100, x_2 = 0$). The directivity pattern is consistent with the computations of Ref. 38 in that the peak sound pressure levels are seen below the mixing layer, centered roughly 30 deg from the horizontal. The acoustic dilatation field was computed and is compared with the results of Ref. 38 in Fig. 12. Because of differences used in forcing the shear layer (Colonius et al.[38] forced the shear layer by oscillating the u_1 velocity at an amplitude of 0.001), a quantitative comparison between EIF and DNS solutions has not been made. However, based on the consistency in the directivity pattern, i.e., both EIF and DNS solutions show a peak directivity roughly 30 deg below $x_2 = 0$, the acoustic field computed using the EIF approach is considered to be in good qualitative agreement with the DNS results. This is significant because fluid–acoustic interaction plays a critical role in processing the acoustic field for this flow and as such validates an important aspect of the EIF approach. The entire solution (hydrodynamic and acoustic fields) using the EIF approach was computed using less than 9 CPU hours on a Cray C90. This is a considerable reduction in time relative to the DNS solution, which required several hundred CPU hours on a Cray Y-MP.[38]

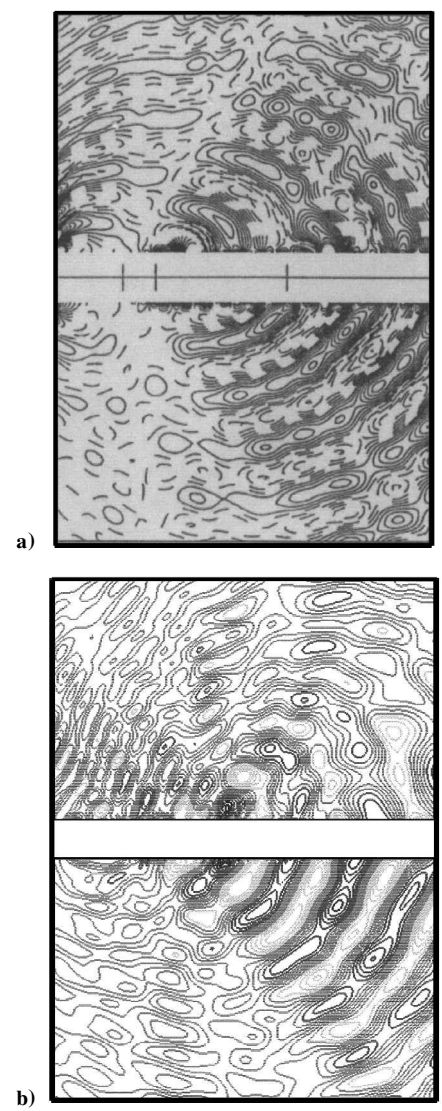

Fig. 12 Shear layer; dilatation field from a) DNS predictions due to Colonius et al.[38] (reprinted with permission of Cambridge University Press), where contour levels range between -0.4×10^{-6} and 0.4×10^{-6} at intervals of 0.04×10^{-6}, and b) EIF predictions, where contour levels range between -0.3×10^{-6} and 0.3×10^{-6} at intervals of 0.03×10^{-6}.

Conclusions

A computational aeroacoustics solver has been developed using the EIF approach. New methods relating the hydrodynamic density to the hydrodynamic pressure, as well as the acoustic pressure to the acoustic and hydrodynamic density, have been used in this solver. In addition, PML absorbing boundary conditions have been implemented to simulate acoustic radiation to the far field. Good agreement with analytical solutions and experimental data has been obtained using the EIF approach for three fundamental validation test cases: the spinning vortex pair, the cylinder in crossflow, and the shear layer. The spinning vortex pair was used to evaluate the PML absorbing conditions. The amplitude and wavelength of the predicted acoustic field is in excellent agreement with a solution obtained using the method of matched asymptotic expansions. Little to no reflection from the PML absorbing region was observed, and the performance of the radiation boundary condition was shown to be relatively insensitive to the amplitude of the PML absorbing coefficients. The cylinder in crossflow was used to demonstrate the complete approach, i.e., computation of the unsteady hydrodynamic flow and the resulting acoustic generation and propagation. This test case showed that the fluid–acoustic interaction terms in the governing equations play a significant role in the prediction of far-field directivity. The computed directivity pattern agrees favorably with experimental results and is strongly influenced by the specified mean hydrodynamic flowfield. Of the three flows considered, the shear layer represents the most difficult test case. The source region associated with this flow is noncompact and, therefore, rigorously tests the ability of the EIF approach in computing flow–acoustic interaction effects. The predicted acoustic field for the shear layer compares quite well with a solution obtained using a fully compressible DNS, verifying an important aspect of the EIF approach. These predictions were obtained at a fraction of the cost of the DNS solutions.

Acknowledgments

The authors would like to acknowledge funding for solver development provided under the Electric Boat Corporation Internal Research and Development program managed by Mark Bennett. Some of the computations were performed under the Numerical Aerodynamic Simulation program.

References

[1]Lighthill, M. J., "Report on the Final Panel Discussion on Computational Aeroacoustics," Inst. for Computer Applications in Science and Engineering, ICASE Rept. 92-53, Hampton, VA, Oct. 1992.

[2]Crighton, D. G., "Computational Aeroacoustics for Low Mach Number Flows," *Computational Aeroacoustics*, edited by J. C. Hardin and M. Y. Hussaini, Springer–Verlag, New York, 1992, pp. 50–68.

[3]Tam, C. K., "Computational Aeroacoustics: Issues and Methods," *AIAA Journal*, Vol. 33, No. 10, 1995, pp. 1788–1796.

[4]Crighton, D. G., "Goals for Computational Aeroacoustics," *Computational Acoustics: Algorithms and Applications*, edited by D. Lee, D. R. L. Sternberg, and M. H. Schultz, *Proceedings of 1st International Association for Mathematics and Computers in Simulation (IMACS) Symposium on Computational Acoustics*, Elsevier Science, New Haven, CT, 1988, pp. 3–20.

[5]Lighthill, M. J., "On Sound Generated Aerodynamically, I. General Theory," *Proceedings of the Royal Society of London*, Vol. A211, No. 1107, 1952, pp. 564–587.

[6]Hardin, J. C., and Pope, D. S., "A New Technique for Aerodynamic Noise Calculation," *Proceedings of the DGLRR /AIAA 14th Aeroacoustics Conference*, AIAA, Washington, DC, 1992, pp. 448–456.

[7]Phillips, O. M., "On the Generation of Sound in Continuous Materials: 2. A Critical Review of the Conceptual Adequacy and Physical Scope of Existing Theories of Aerodynamic Noise, with Special Reference to Supersonic Jet Noise," *Journal of Sound and Vibration*, Vol. 25, No. 2, 1972, pp. 263–335.

[8]Lilley, G. M., "On the Noise from Jets," CP-131, AGARD, 1974.

[9]Goldstein, M. E., *Aeroacoustics*, McGraw–Hill, New York, 1976, pp. 253, 254.

[10]Hardin, J. C., and Pope, D. S., "Sound Generation by a Stenosis in a Pipe," AIAA Paper 90-3919, Oct. 1990.

[11]Lee, D. J., and Koo, S. O., "Numerical Study of Sound Generation Due to a Spinning Vortex Pair," *AIAA Journal*, Vol. 33, No. 1, 1995, pp. 20–26.

[12]Slimon, S. A., Soteriou, M. C., Davis, D. W., and Hardin, J. C., "Development of Computational Aeroacoustic Equations for Subsonic Flows Using a Mach Number Expansion Approach," *Journal of Fluid Mechanics* (submitted for publication).

[13]Slimon, S. A., and Davis, D. W., "Computational Prediction of Secondary Flows in Complex Piping Systems," *Advances in Computational Methods in Fluid Dynamics*, Vol. 196, American Society of Mechanical Engineers, Fluids Engineering Div., New York, 1994, pp. 393–403.

[14]Slimon, S. A., Davis, D. W., Levinson, S., Krane, M., Richard, G., Sinder, D., Duncan, H., Lin, Q., and Flanagan, J., "Low Mach Number Flow Through a Constricted Stylized Vocal Tract," AIAA Paper 96-1734, May 1996.

[15]Wagner, C. A., Davis, D. W., Slimon, S. A., Languedoc, R. M., and Hollingsworth, T. A., "Calculations of Submarine Free Surface Flows Using a Highly Efficient and Mature Reynolds Averaged Navier–Stokes Solver," *Proceedings—Third International Symposium on Performance Enhancement for Marine Applications*, U.S. Naval Undersea Warfare Center, Div. Newport, Newport, RI, 1997, pp. 1–9.

[16]Rogers, S. E., Kwak, D., and Kiris, C., "Steady and Unsteady Solutions of the Incompressible Navier–Stokes Equations," *AIAA Journal*, Vol. 29, No. 4, 1991, pp. 603–610.

[17]MacCormack, R. W., "A Numerical Method for Solving the Equations of Compressible Viscous Flow," AIAA Paper 81-0110, Jan. 1981.

[18]Berenger, J.-P., "A Perfectly Matched Layer for the Absorption of Electromagnetic Waves," *Journal of Computational Physics*, Vol. 114, 1994, pp. 185–200.

[19]Hu, F. Q., "On Perfectly Matched Layer as an Absorbing Boundary Condition," AIAA Paper 96-1664, May 1996.

[20]Mitchell, B. E., Lele, S. K., and Moin, P., "Direct Computation of the Sound From a Compressible Co-Rotating Vortex Pair," *Journal of Fluid Mechanics*, Vol. 285, 1995, pp. 181–202.

[21]Müller, E.-A., and Obermeier, F., "The Spinning Vortices as a Source of Sound," CP-22, AGARD, 1967, pp. 22.1–22.8.

[22]Blake, W. K., *Mechanics of Flow-Induced Sound and Vibration Volume 1. General Concepts and Elementary Sources*, Academic, London, 1986, pp. 214–220.

[23]Tam, C. K., and Hardin, J. C. (eds.), *Second Computational Aeroacoustics (CAA) Workshop on Benchmark Problems*, NASA CP-3352, June 1997, p. 8.

[24]Revell, J. D., Prydz, R. A., and Hays, A. P., "Experimental Study of Airframe Noise vs. Drag Relationship for Circular Cylinders," Lockheed Rept. 28074, Final Rept. NASA Contract NAS1-14403, Feb. 1977.

[25]Brentner, K. S., Cox, J. S., Rumsey, C. L., and Younis, B. A., "Computation of Sound Generated by Flow over a Circular Cylinder: An Acoustic Analogy Approach," *Second Computational Aeroacoustics (CAA) Workshop on Benchmark Problems*, NASA CP-3352, June 1997, pp. 289–296.

[26]Kumarasamy, S., Korpus, R., and Barlow, J. B., "Computation of Noise Due to Flow over a Circular Cylinder," *Second Computational Aeroacoustics (CAA) Workshop on Benchmark Problems*, NASA CP-3352, June 1997, pp. 297–304.

[27]Spyropoulos, E. T., and Holmes, B. S., "Large Eddy Simulation of a High Reynolds Number Flow Around a Cylinder Including Acoustic Predictions," *Second Computational Aeroacoustics (CAA) Workshop on Benchmark Problems*, NASA CP-3352, 1997, pp. 319–328.

[28]Curle, N., "The Influence of Solid Boundaries Upon Aerodynamic Sound," *Proceedings of the Royal Society of London*, Vol. A231, No. 1187, 1955, pp. 505–514.

[29]Ffowcs Williams, J. E., and Hawkings, D. L., "Sound Generated by Turbulence and Surfaces in Arbitrary Motion," *Philosophical Transactions of the Royal Society*, Vol. A264, No. 1151, 1969, pp. 321–342.

[30]Brown, G. L., and Roshko, A., "On Density Effects and Large Structures in Turbulent Mixing Layers," *Journal of Fluid Mechanics*, Vol. 64, 1974, pp. 775–816.

[31]Browand, F. K., and Weidman, P. D., "Large Scales in the Developing Mixing Layer," *Journal of Fluid Mechanics*, Vol. 76, 1976, pp. 127–144.

[32]Ho, C. M., and Huang, L. S., "Subharmonics and Vortex Merging in Mixing Layers," *Journal of Fluid Mechanics*, Vol. 119, 1972, pp. 443–473.

[33]Corcos, G. M., and Sherman, F. S., "The Mixing Layers: Deterministic Models of a Turbulent Flow, Part I, Introduction and the Two-Dimensional Flow," *Journal of Fluid Mechanics*, Vol. 139, 1984, pp. 29–65.

[34]Grinstein, F. F., Oran, E. S., and Boris, J. P., "Numerical Simulations of Asymmetric Mixing in Planar Shear Flows," *Journal of Fluid Mechanics*, Vol. 165, 1986, pp. 201–220.

[35]Ghoniem, A. F., and Ng, K. K., "Numerical Study of the Dynamics of a Forced Shear Layer," *Physics of Fluids*, Vol. 30, No. 3, 1987, pp. 706–721.

[36]Laufer, J., and Yen, T., "Noise Generation by a Low-Mach Number Jet," *Journal of Fluid Mechanics*, Vol. 134, 1983, pp. 1–31.

[37]Crighton, D. G., and Huerre, P., "Shear-layer Pressure Fluctuations and Superdirective Acoustic Sources," *Journal of Fluid Mechanics*, Vol. 220, 1990, pp. 355–368.

[38]Colonius, T., Lele, S. K., and Moin, P., "Sound Generation in a Mixing Layer," *Journal of Fluid Mechanics*, Vol. 330, 1997, pp. 357–409.

[39]Soteriou, M. C., and Ghoniem, A. F., "Effects of the Free-Stream Density Ratio on Free and Forced Spatially Developing Shear Layers," *Physics of Fluids*, Vol. 7, No. 8, 1995, pp. 2036–2051.

P. J. Morris
Associate Editor